https://doi.org/10.5194/egusphere-2024-659
Preprint. Discussion started: 19 April 2024


# Using UAV-Derived Point Clouds to measure high resolution cliff dynamics in soft lithologies: Demons Bluff, Victoria, Australia

Todd A. Doran[1], David M. Kennedy[2], R. Jak McCarroll[3], Blake M. Allan[3], and Daniel Ierodiaconou[1]

[1] School of Life and Environmental Sciences, Deakin University, Warrnambool Campus, Warrnambool, 3280, Australia
[2] School of Geography, Earth & Atmospheric Sciences, The University of Melbourne, Parkville, 3010, Australia
[3] Department of Energy, Environment, and Climate Action, East Melbourne, Victoria 3002, Australia

*Corresponding Author*: Todd A. Doran, email: t.doran@deakin.edu.au

**Abstract**

Unoccupied aerial vehicles (UAVs) have revolutionised data collection on the Earth's surface. Through aerial photogrammetry, very high-resolution digital surface models can be produced enabling contemporary research on landscape stability. There are however significant limitations in the imaging of vertical and overhanging landforms when using aerial platforms for data collection. Rather than reconstructing change from a digital surface model, direct analysis of generated point clouds is likely the key for understanding landform change in these morphologically complex environments. In this study, UAV's were used to collect aerial imagery generating a high spatio-temporal resolution timeseries comprising of thirty point cloud datasets spanning four years for the steeply sloped Demons Bluff cliff located on the Great Ocean Road, Victoria, Australia. A method was developed to analyse the large quantity of 3D point cloud datasets. It was then possible to capture changes in cliff face morphology, enabling us to enhance our understanding of the erosional processes in coastal cliff environments. Over the study, the retreat rate for the upper half of the cliff face was 0.67 m/year (0.60 $m^3$/m/yr). Cliff erosion was found to be dominated by 9 high magnitude, cliff-top collapses that exceeded 1,000 $m^3$ (up to 9,500 $m^3$) and terminated mid-way down the cliff. Below this point, several slab detachments were observed. Pre-collapse deformation was detected before collapses > 300 $m^3$ with success (75 % of the time) in areas with a complete timeseries over the four-year period. Deformation was observed to occur in two ways, and both were observed to be eventuate in high magnitude (> 1,000 $m^3$) collapse. The first which occurred prior to most high magnitude collapses (> 500 $m^3$) was caused by the expansion of tension cracks behind the cliff-top, and the second which was characterised by smaller collapse volumes (> 100-500 $m^3$) was initiated by rock slabs fracturing and cleaving away from the cliff face and was proceeded by high magnitude failure (< 1000 $m^3$). An additional 14 instances of lean have been identified that are yet to result in collapse and should continue to be monitored to assess the success of this method with the forecasting of future collapse locations. Ultimately, this provides the ability to identify potential locations for future collapses which could aid in the development of an early warning system for cliff collapse to improve the management of volatile cliff environments that pose threats to infrastructure and public safety.

## 1. Introduction

Cliffs are prominent landforms that comprise ~52 % of coastlines globally (Young and Carilli, 2019). Projections for sea level rise and Changed intensity and frequency of storms is forecast to enhance future rates of cliff recession (Limber et al., 2018, Lim et al., 2010). This has implications for coastal planning and public safety, signifying a need to better understand the processes of cliff retreat and identify the environmental drivers of morphometric change in cliff landscapes.

Quantitative methods to analyse cliff change advanced over the past few decades. Methods of data capture have evolved from ground-based physical field survey using levels and theodolites (Smith and Zarillo, 1990), to comparison of satellite imagery or cartographic charts (Bray and Hooke, 1997), terrestrial photogrammetry (Gulyaev and Buckeridge, 2004), terrestrial and

https://doi.org/10.5194/egusphere-2024-659
Preprint. Discussion started: 19 April 2024


aerial laser scanning (Dewez Thomas et al., 2013, Young et al., 2014), with Unoccupied Aerial Vehicles (UAVs) surveys now becoming a more common approach (Esposito et al., 2017). Of these methods, the LiDAR-based aerial and terrestrial laser scanning have dominated cliff erosion studies in the past decade (Letortu et al., 2018, Rohmer and Dewez, 2013, Theodore et al., 2020, Young et al., 2009, Terefenko et al., 2019, Bezore et al., 2019, Katz and Mushkin, 2013), owing to their ability to produce 3D point clouds (hereafter denoted as "point clouds") that allow visualisation and analysis of landscapes in three dimensions. More recently, UAVs with the ability to collect Structure from Motion (SfM) photogrammetry have provided a cost-effective way to collect data with high spatial resolution and capability to produce point clouds (Mancini et al., 2017, Dewez Thomas et al., 2013), thereby allowing for the generation of extensive multi-temporal datasets (Ierodiaconou et al., 2022).

Despite the truly three-dimensional nature of point cloud datasets, it is more common for geomorphic analysis to be performed using digital elevation models (DEM) that are a derived product from the point cloud. The downside of DEMs is that they are pseudo-3D and have a limited ability to visualise and measure change across vertical and undercut surfaces (Lague et al., 2013, Li et al., 2021). However, the analysis of point clouds overcomes these limitations and provides the ability to accurately measure change and describe erosion processes. For example, Alessio and Keller (2020) utilised point clouds for five small (< 145 m width) coastal cliffs in Santa Barbara, California. They found retreat of cliff toe occurred first, with the middle and upper portions of cliff eroding back at a later time until they patched the position of the toe, whereby the cycle would reinitiate. As illustrated by Hendrickx et al. (2022), point clouds can also be used to detect the precursory deformation on rock walls prior to major collapse in mountainous landscapes. In Matter Valley, Switzerland, the changes in point clouds allowed identification of rock slabs cleaving, which resulted in debris falls that eventually lead to more major collapse of larger areas. Similarly, Abellan et al. (2010) at Pallars Jussà, Spain, identified areas of deformation prior to small rockfall event and measured a maximum horizontal displacement value that could be used to predict the locations of future collapses. However, few studies have utilised an extensive timeseries of point clouds generated solely by UAV photogrammetry to analyse cliff retreat and to our knowledge, there has been limited application to determine whether such approaches can identify pre-collapse deformation.

Despite the highlighted upsides of point cloud analysis, a methodology is yet to be developed for an ongoing temporal analysis of point clouds for a single steep coastal cliff containing high quantities (> 20) of UAV generated datasets. A higher spatio-temporal resolution of analyses is important for informing management decisions surrounding rockfall hazards, or localised measures of cliff top retreat. This study aims to develop a methodology for the analysis of large datasets of near vertical coastal cliffs. It utilised a unique citizen-scientist UAV dataset (Ierodiaconou et al., 2022) collected bimonthly over four years along > 1.5 km of coast to test the ability of point clouds to detect meaningful change in coastal cliffs along a high-energy open-coast.

## 2. Methodology

### 2.1 Site Description

Demon's Bluff (-38.405, 144.204) is found on the exposed southern coast of Australia (Fig. 1(a, b, c)). The 1.5 km long cliffs are formed within the Eocene-Oligocene Demon's Bluff formation (Shalaby et al., 2020). This is a calcareous sand to mud-sized unit with interbeds of coal and other fine-grained terrestrial units. The cliff face is divided into two units, an upper yellow and lower greyish unit, the boundary lying approximately halfway up the cliff. The precise chemical and sedimentological differences between the units are unknown. The cliff rises 30 - 50 m in height from the intertidal zone. It is fronted by a low-gradient, dissipative intertidal sandy beach up to 90 m wide at low tide but the cliff toe experiences wave actions during high tide (Ierodiaconou et al., 2022). Tides are semidiurnal and microtidal. The deep-water wave climate is seasonal where the maximum significant waves heights are greatest during winter (~ 4 m) and year-round average peak wave periods exceed 11 seconds (Liu et al., 2022). The region has a temperate climate, receiving a mean annual precipitation of 631 mm, the majority of which falls through winter and early spring.

https://doi.org/10.5194/egusphere-2024-659
Preprint. Discussion started: 19 April 2024


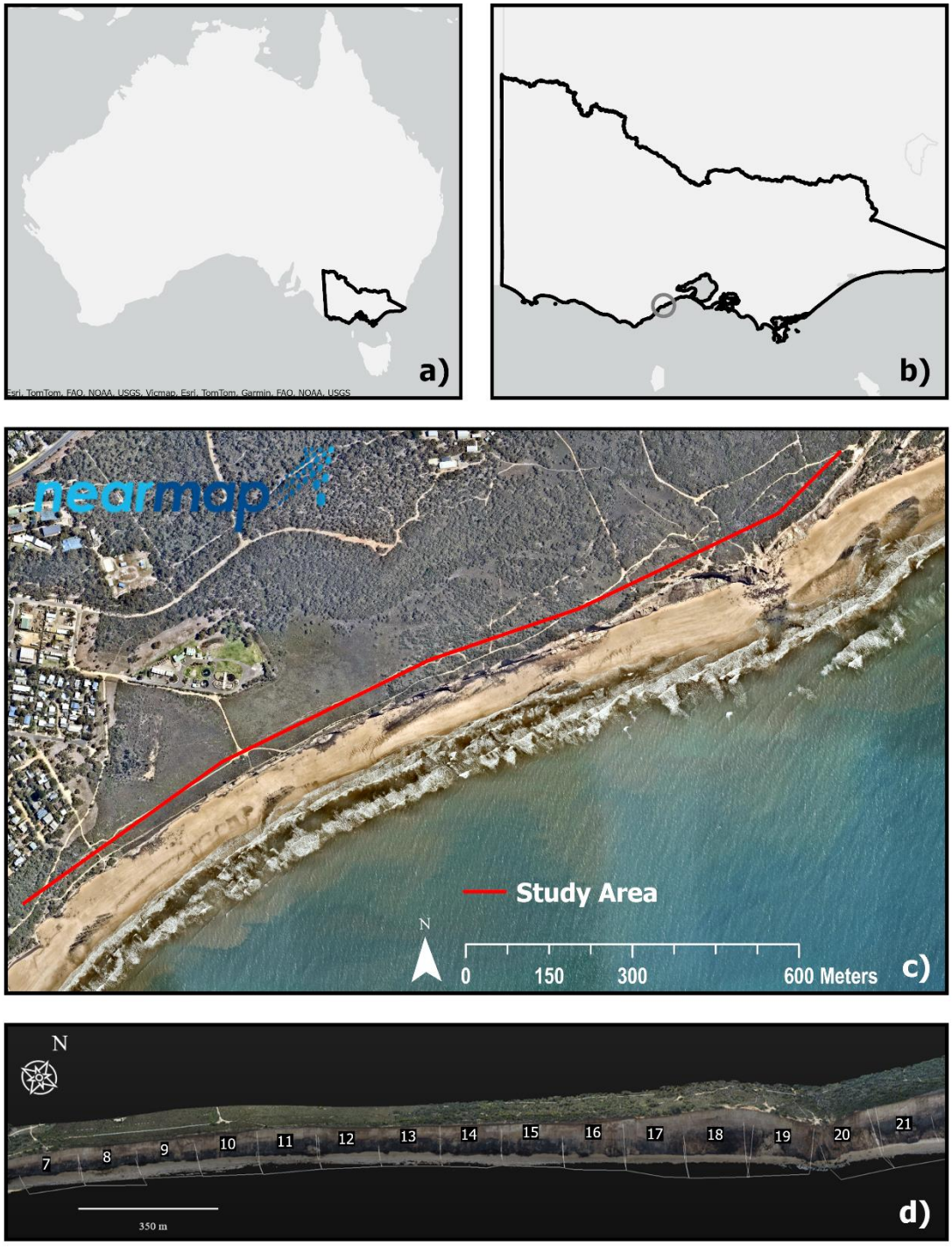


**Fig. 1:** a,) Location of Demons Bluff within Australia, b) Location of Demons Bluff within Victoria, Overview of the site, c) Overview of the study area (Imagery: Nearmap), d) Oblique view of Demons Bluff showing section numbers. Site maps were generated using ArcGIS Pro 3.1.1, Redlands, CA, USA.

https://doi.org/10.5194/egusphere-2024-659
Preprint. Discussion started: 19 April 2024


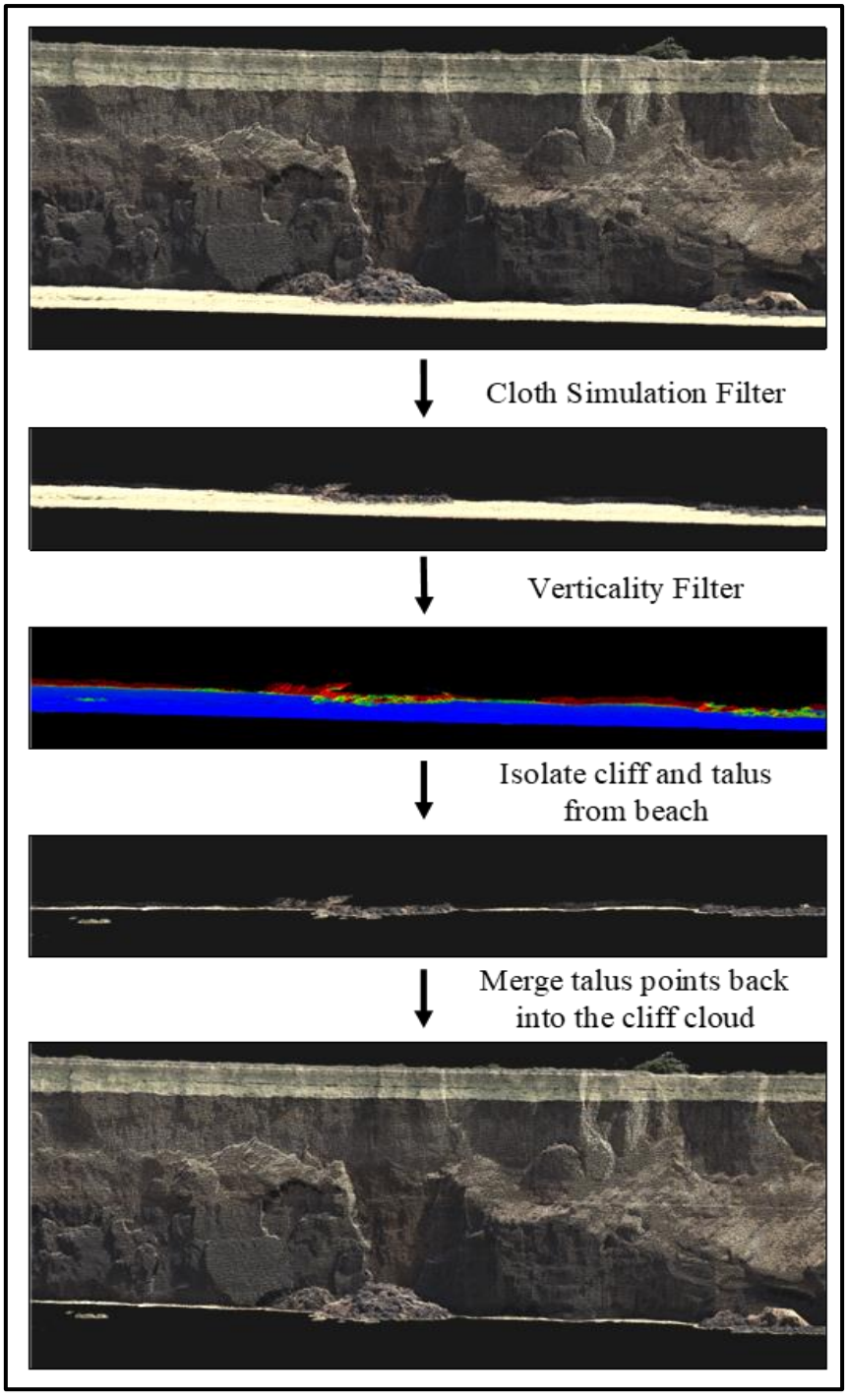


**Fig. 2:** Flow diagram outlining the process used to isolate the cliff face and talus from the fronting beach.

https://doi.org/10.5194/egusphere-2024-659
Preprint. Discussion started: 19 April 2024


## 2.2 Point Cloud Workflow

Data collection was undertaken using DJI Phantom P4 and RTK models, as per Ierodiaconou et al. (2022) and Pucino et al. (2021). Point clouds derived from the drone imagery were georeferenced with an average total error of 40 mm and had an average ground sampling distance of 23 mm.

Point cloud analysis was undertaken in CloudCompare V.2.12.1 (Cloudcompare, 2022). Point clouds were manually filtered to remove areas landward of the cliff top, and subsequently, the cloud was processed with the Cloth Simulation Filter (CSF) developed by Zhang et al. (2016) to isolate the cliff face from the fronting beach. CSF inverts the point cloud (flipping by 180°) and projects a cloth over the underside of the terrain. If an area of terrain deviates from the cloth, it is identified as a non-ground point. This created separate beach and cliff point clouds by classifying the beach as ground points and the cliff as non-ground points. Some regions of cliff and talus were misclassified as beach (Fig. 2). This was resolved by using the "verticality" tool in CloudCompare that quantifies the slope of a surface. Incorrectly classified areas of cliff face and talus are more vertical than the beach and returned higher values of verticality, allowing them to be identified and reclassified as cliff points. Each cloud was assessed for miss-classified points, typically boulders on the beach and talus with a gradual slope (< 10 º) which were then manually segmented and reclassified. The verticality filter was then applied to the cliff cloud to reduce the density of cliff-top vegetation, which permitted the accurate manual tracing and removal of all points on the landward side of the cliff edge. The cliff and beach were segmented every 100 m in an alongshore direction to allow the identification of hotspots for retreat and to retain the ability to detect incremental change (Fig. 1(d)) which tends to be lost when analysing longer sections of coast (Neverman et al., 2016). Due the cliff geology, 100 m sections were further divided in half, vertically, to investigate the behaviour of the two different units (Fig. 3). Cliff volumetric change measurements were performed using a raster projected from the x-axis in an across-shore direction. Each section was aligned perpendicularly to the x-axis to ensure optimal raster coverage over the cliff face.

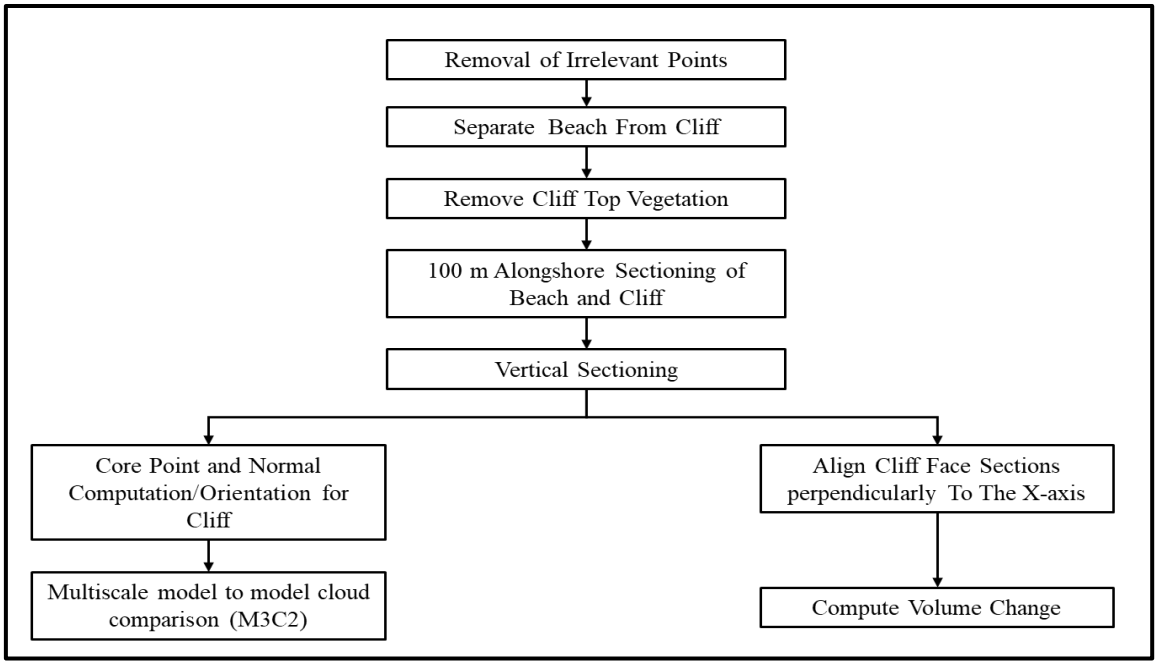


**Fig. 3:** A schematic overview of the developed methodology for point cloud analysis undertaken in CloudCompare v2.12.

https://doi.org/10.5194/egusphere-2024-659
Preprint. Discussion started: 19 April 2024


115

### 2.2.1 Change Detection

Volumetric change was estimated using the "Compute 2.5D Volume" tool in CloudCompare that was set to project a 0.15 x 0.15 m raster from the x-axis onto the cliff face. Rasters were set to interpolate over areas of occlusion. Downfalls of using rasters in cliff analyses, such as their inability to portray and measure change across vertical surfaces (Lague et al., 2013, Li et al., 2021) and the interpolation over surface occlusions that often arise in complex, non-linear regions of cliff (Esposito et al., 2017, Scaioni et al., 2013) were overcome by projecting the raster onto the cliff face from the x-axis, rather than the z-axis. This removes the limitation of being unable to visual and measure change across vertical and sub-vertical cliff faces. Error associated with interpolation was minimised by the absence of occlusions on the cliff face and the relatively simple geometry of the cliff.

The M3C2 algorithm developed by Lague et al. (2013) was used to measure the 3D distance change in cliff face position. It measures change along surface normals that extend from core points in a reference cloud. The position of a core point is defined by the average position of points within a set radius on the reference cloud. The normals extend outwards from the core points and follow the orientation of the cloud's surface. A cylinder of a set radius and depth is projected in the direction of the normal around each core point and traverses both the reference and compared clouds. Within each cylinder is a subset of points from the reference cloud, *n1*, and the compared cloud, *n2*. M3C2 then measures the average difference in the position of the two subsets of points to calculate the distance change within that cylinder (Fig. 4). Each cylinder generates a 95% confidence interval for the measured change that considers uncertainty in surface position caused by noise, registration error between the two clouds, and variability in surface roughness caused by differential scanner/camera positions. Distance and volumetric change estimates were calculated for each section by comparing a cliff point cloud in the same section from the previous survey.

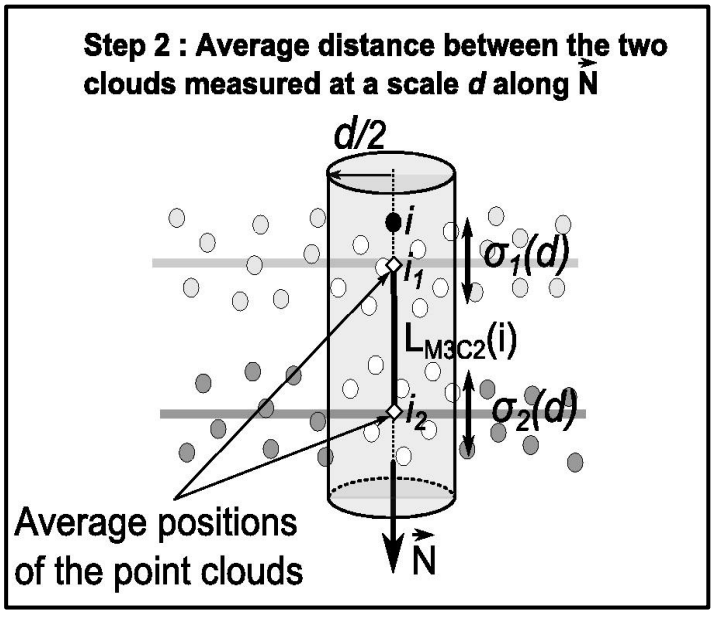


**Fig. 4:** Calculation of the average surface positions created by points within the defined radius (D/2) and calculation of M3C2 distance along the direction of the core points (i) normal (N). Adapted from Lague et al. (2013).

https://doi.org/10.5194/egusphere-2024-659
Preprint. Discussion started: 19 April 2024


140

## 3. Results

### 3.1 Performance of Point Cloud Workflow

From segmenting the upper and lower regions of the cliff, the ability to measure the volumetric change in upper and lower parts of the cliff was enabled. This also allowed the quantification of talus deposition and erosion following failure higher in
145 the cliff. Using the point cloud method, this talus could not be directly analysed as a separate geomorphic entity but is measured as a change in the lower half of the cliff. The accumulation of talus is still well represented by a direct correlation (p-value = <0.05, $r^2$ = 0.35) between upper cliff loss and subsequent lower cliff deposition (Fig. 5). On average, a limit of detection of 71 mm was measured across the study, with a minimum LOD of 60 mm and a maximum of 90 mm. Error assessment for volumetric change was carried out by comparing the position of a surface that did not change between surveys. A concrete
150 boat ramp that was located within the survey area was used as a reference surface and volumetric change comparisons were undertaken between each survey. On average, there was found to be an error of 1.3 $m^3$ / 100 $m^2$. On average, this equated to a mean error of +/- 46 $m^3$ (0.46 $m^3$/m) (lower cliff = 22 $m^3$, upper cliff = 24 $m^3$) across each 100 m section (mean SA = 3522 $m^2$) and permitted the identification of 298 erosional events. If volumetric assessment was undertaken on a cliff-wide scale, the mean error would be, on average +/- 302 $m^3$ (SA = 23,092 $m^2$) and be as high as +/- 751 $m^3$ (SA = 57,508 $m^2$) in surveys
155 that contained the greatest extent of the cliff.

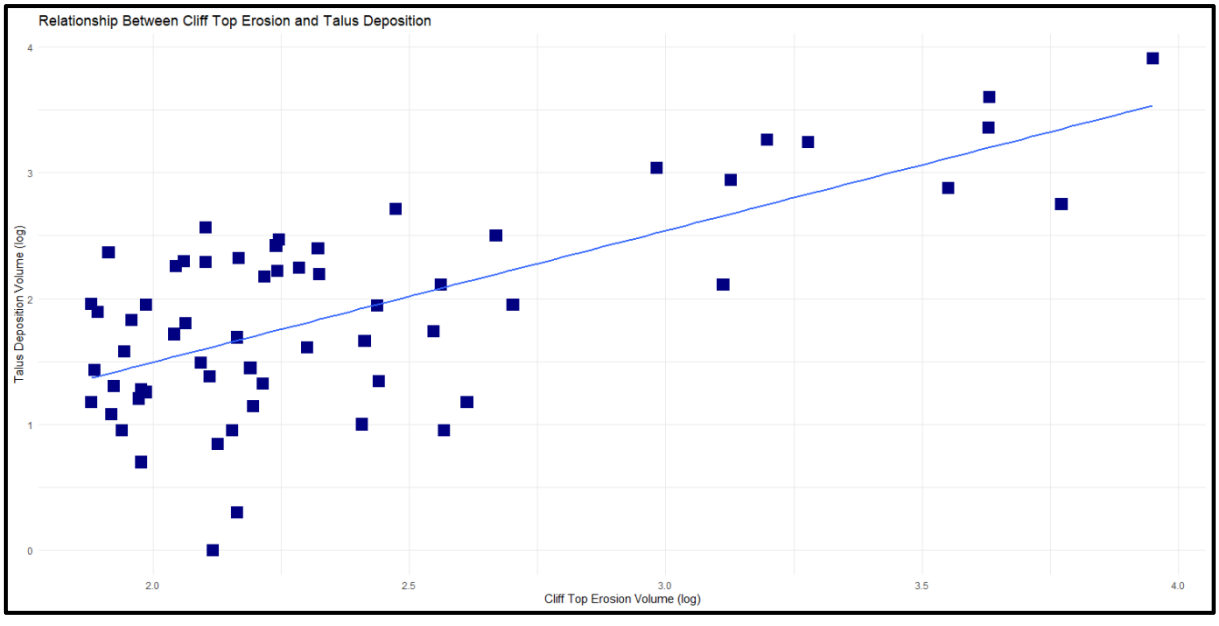


**Fig. 5:** Scatterplot showing the correlation between magnitudes of lower cliff deposition (y) following cliff top erosion (x)

https://doi.org/10.5194/egusphere-2024-659
Preprint. Discussion started: 19 April 2024


### 3.2 Trends of Cliff Erosion

From June 2018 to August 2022, the mean retreat rate for the upper half of the cliff was 0.67 m/yr (~11,000 $m^3$/year) equating to a loss of 46,300 $m^3$ (1.53 $m^3/m^2$, 2.5 $m^3$/m alongshore, 0.60 $m^3$/m/yr) across the entire extent of the upper cliff face. Erosion of upper cliff was dominated by infrequent, high magnitude events. High magnitude cliff top collapse typically occurred where tension cracks had opened within 10 m landward of the cliff edge. Over time, cracks widened and caused seaward tilting of the upper cliff (Fig. 6(a, *i*)). Large-scale cliff top failure (> 1000 $m^3$) rarely encompassed the entire cliff face except for the collapse in Fig 6(a, *ii*)) and typically terminated just above the mid-cliff point at the contact between the two rock units. The failure plane now exposed as a result of the rocky fall was more gradual in slope (55–70 °) than the surrounding cliff (~ 85-90 °). Slabs of rock that spanned the bottom two-thirds of the cliff were observed to fracture and separate away from the cliff face and cause infrequent, moderate magnitude detachments (~ 100-400 $m^3$) (Fig. 6(b, *ii*)). This saw the incline of the cliff face where the failure plane existed to become steeper and less pronounced until the cliff face returned to being near-vertical (Fig. 7). Slab detachment in the mid cliff (Fig. 6(b, *ii*)) also suggests that failure in this location may have some influence in the trigger of larger collapse, as tension cracks were absent above the section that failed in the following survey (Fig. 6(b, *iii*)). In total, nine events occurred where over 1,000 $m^3$ was lost from the upper cliff (Fig. 8), which accounted for ~ 71% of total upper cliff erosion over the 50 months of monitoring. The largest event which caused the greatest retreat of the cliff top (mean of 3.47 m over the entire section) had a volume of 9,500 $m^3$. Upper cliff erosion occurred within spatial and temporal hotspots (Fig. 9). Due to variations in the extent of the survey alongshore, only sections 7 - 11 appeared in surveys between May-June within each year. These areas were therefore used to identify if retreat rates, and hotspot locations fluctuated between years. Prior to May 2020, the overall mean upper cliff retreat rate was 0.32 m/yr. However, the retreat rate was driven by a single hotspot within section ten (1.54 m/yr) as retreat in other sections was negligible (0.02 m/year) (Fig. 9(a)). In the following 12-months, three of the five sections recorded upper cliff rates of retreat that exceeded 1 m/year. This resulted in a mean upper cliff retreat rate almost three times higher than previously recorded, at 0.92 m/yr. In 2022, retreat rates have declined to 0.28 m/yr. Cumulative retreat exceeding two meters over the entire 100 m section was observed in four sections (Fig. 9(b)). Of those, section ten receded the farthest, with an average cumulative retreat of 4.7 m across the 100 m section. Erosion within this section of cliff mostly occurred from three separate, high magnitude events involving upper cliff erosion volumes of 960 $m^3$, 4,200 $m^3$, and 1,900 $m^3$. Other upper cliff sections with cumulative retreats exceeding 2 m were attributed to single events as no other erosional event > 300 $m^3$ was observed prior to, or after, the high magnitude collapses. The relationship between upper cliff loss and lower cliff accumulation is not equal. Of the total mass lost from the upper cliff, 79.9 % (37,000 $m^3$) was deposited in the lower cliff area. This indicates that 20 % (~ 9,000 $m^3$) of talus was eroded between collapse and the succeeding survey. This is observed in rates of deposition on the lower cliff following similar trends (r = 0.59) as upper cliff erosion (Fig.8) but is typically of a lower magnitude.

The overall extent of erosion for the lower cliff, which includes the cliff itself and the talus mantled on its face, exceeded 77,000 $m^3$ over the 50 months of survey. Erosion episodes in the area comprised mostly of high frequency, low-magnitude (< 200 $m^3$) events but experienced larger episodic anomalies following talus deposition on the cliff base and slab detachments that encompassed the mid-cliff junction (Fig. 8), particularly when collapses coincided with high energy wave conditions and talus deposits were completed eroded across several survey intervals.

https://doi.org/10.5194/egusphere-2024-659
Preprint. Discussion started: 19 April 2024


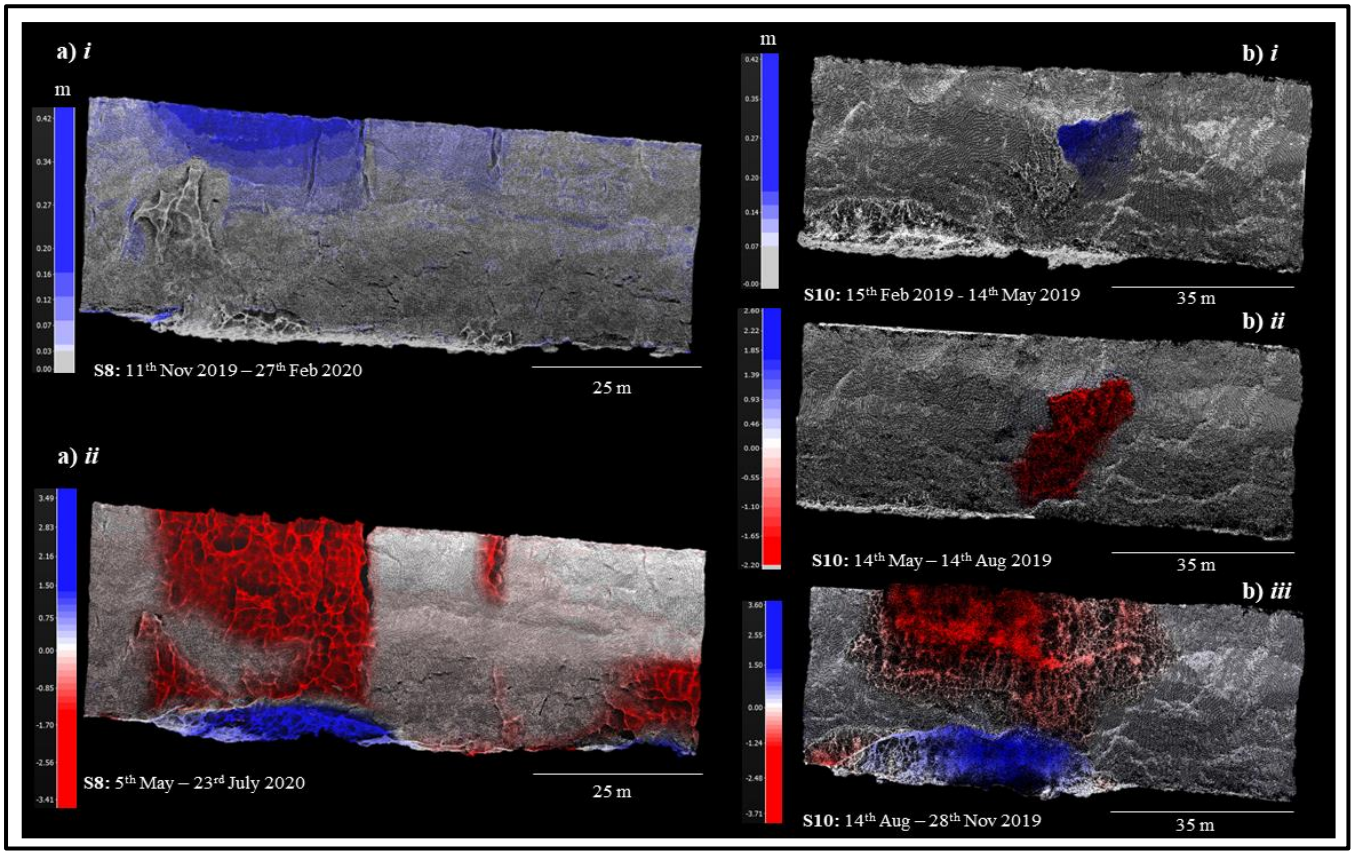


**Fig. 6 (above):** M3C2 distance change output clouds showing **a)** Seaward cliff top lean (**i**)), resulting in a collapse of 1330 $m^3$ (**ii**)). **b)** The progression of a slab leaning (**i**)), detaching (**ii**)), and being followed by high magnitude cliff top failure (**iii**)) with a volume of 4580 $m^3$.
**Fig. 7 (below):** Schematic flow diagram illustrating the dominant erosion process observed at Demons Bluff throughout this study.

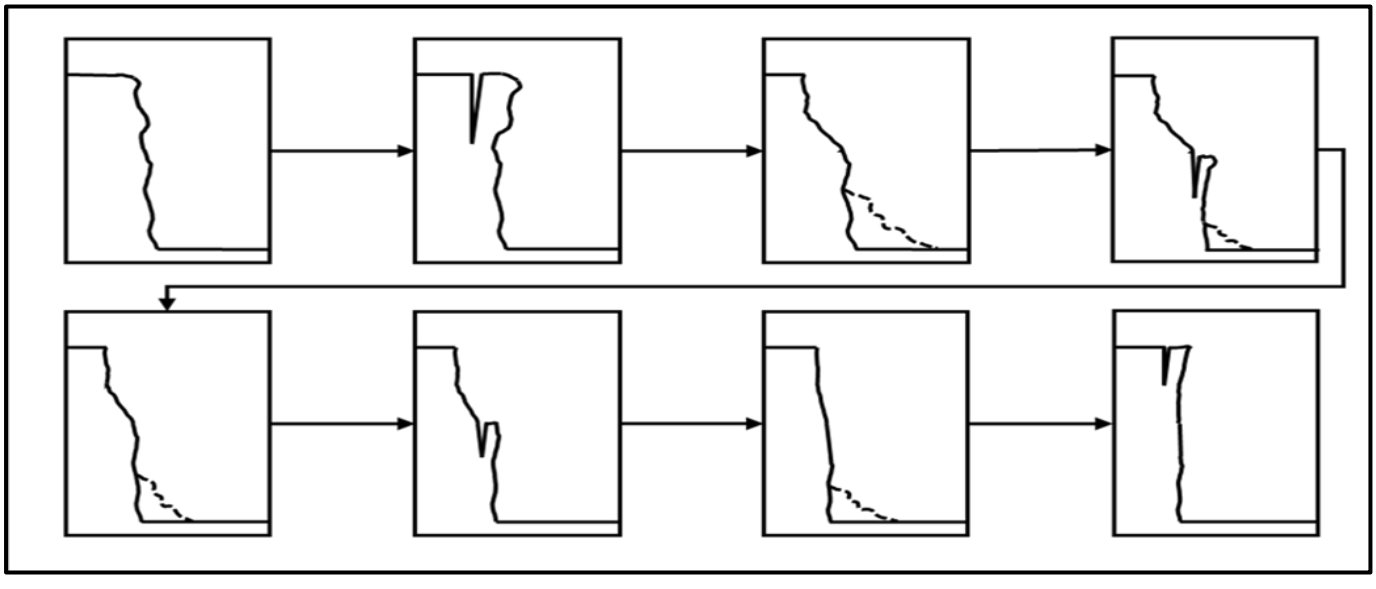

https://doi.org/10.5194/egusphere-2024-659
Preprint. Discussion started: 19 April 2024


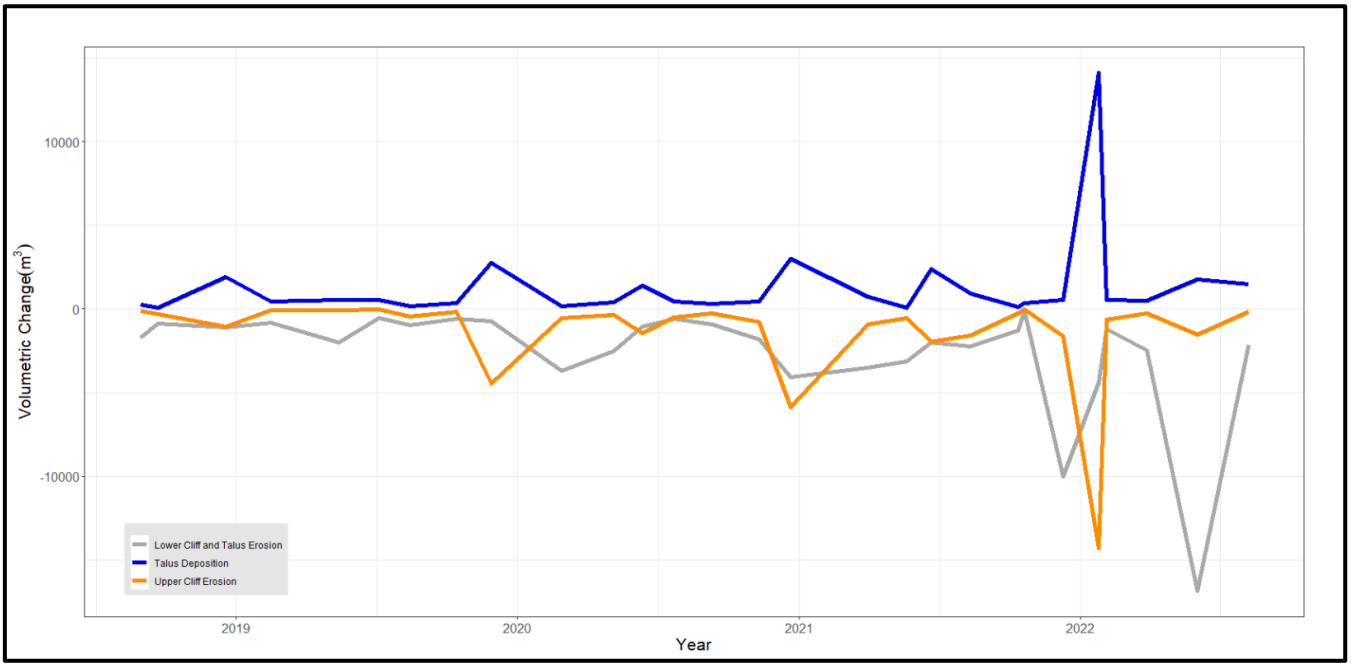


**Fig. 8:** Timeseries that illustrates the patterns of erosion and deposition experienced across the upper and lower regions of cliff at Demons Bluff at throughout every survey interval.

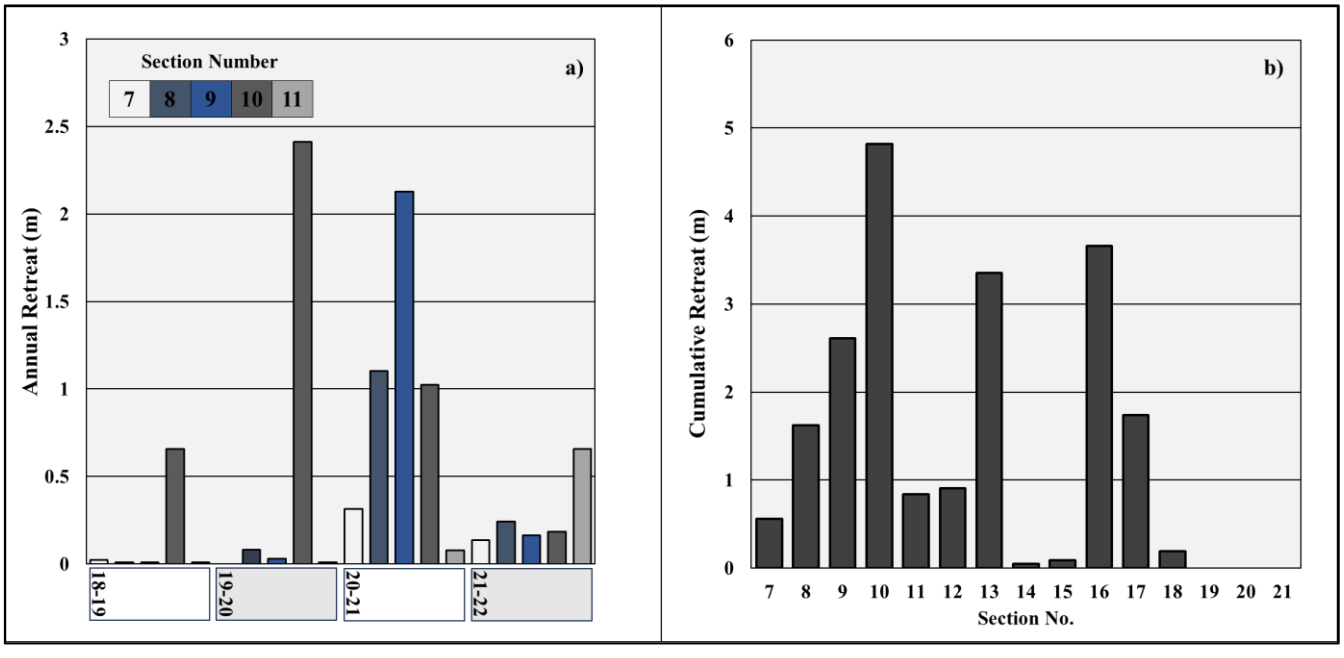


**Fig. 9: a)** Annual upper cliff rates of retreat for Sections 7 - 11 for each 12-month period throughout the study duration. **b)** The average cumulative cliff top retreat for each 100 m section over the duration of the study.

205

https://doi.org/10.5194/egusphere-2024-659
Preprint. Discussion started: 19 April 2024


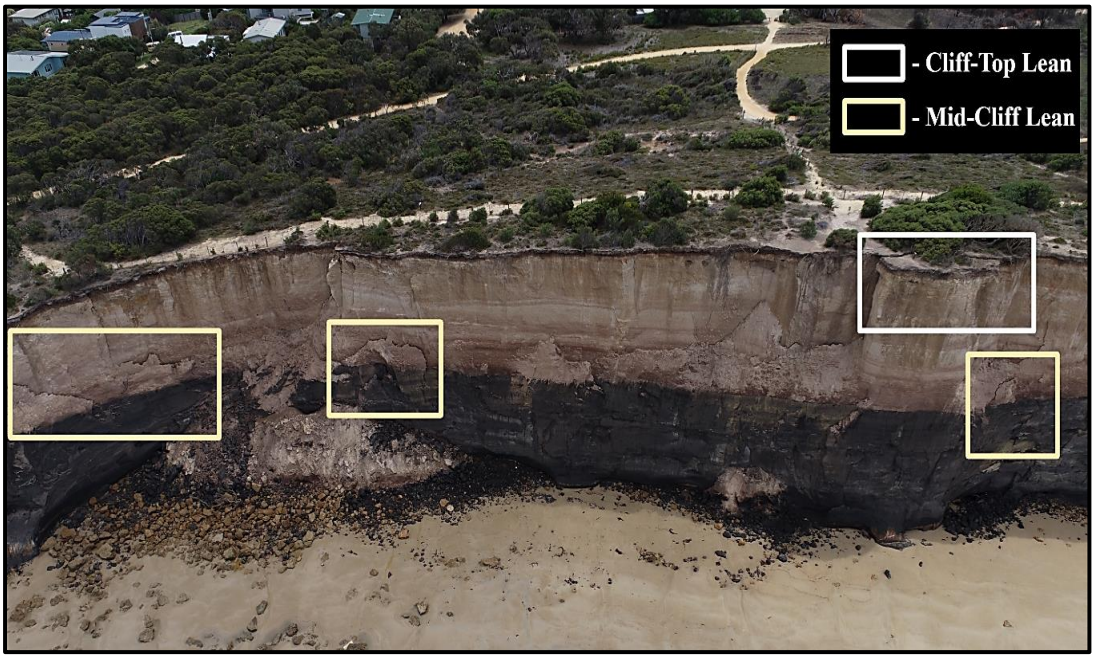


**Fig. 10:** Field photograph showing areas of slab detachment in the mid-cliff (yellow) and the expansion of tension cracks causing cliff-top lean (white).

### 3.3 Mechanism of Collapse

The resolution of the points clouds at Demons Bluff, allowed measurement of the physical preconditions to cliff collapse to be made. This is observed in apparent accretion of the cliff top through the point cloud analysis. In the field, tension cracks behind the cliff top could be seen expanding and cause the upper half of the cliff to displace itself outwards toward the sea and ultimately result in high magnitude cliff failure. Slabs of rock lower on the cliff were also observed to fracture and slowly separate away from the cliff face (Fig. 10) and eventually cause infrequent, moderate magnitude detachments (Fig. 6(b, ii)). This saw the cliff face that formed from the failure plane to become steeper and less pronounced until the slope returned to being near-vertical (Fig. 7). Slab detachment within the mid cliff (eg. Fig. 6(b, ii)) may be a factor in cliff destabilisation and contribute as a trigger for larger collapse. In the instance in Fig. 6(b), tension cracks that were observed prior to other high magnitude collapses were absent and failure occurred in the survey period following a slab detachment encompassing the lower-mid cliff. (Fig. 6(b, iii)).

Given that sections 7 – 11 appeared to possess adequate temporal resolution for lean detection, this provided the ability to explore whether lean events had occurred prior to smaller collapses (> 300 $m^3$). From this, it was identified that incremental lean occurs over many surveys, and not just immediately prior to a single failure. In total, eight cliff collapse events occurred where over 300 $m^3$ was lost from the upper cliff between section 7 – 11. Of these eight events, cliff lean was identified in the M3C2 output cloud prior to six, a coincidence rate of 75 %. The only instances when collapse was not preceded by lean occurred for a collapse (960 $m^3$) that occurred in the third survey of the dataset. It is possible however, that lean had occurred but was not recorded as the cliff failure was 3 – 6 months after the first survey in this study. The other collapse (3558 $m^3$) that did not display lean or tension cracks in the cliff top was found adjacent to an area that had collapsed (1341 $m^3$) a year earlier.

https://doi.org/10.5194/egusphere-2024-659
Preprint. Discussion started: 19 April 2024


By comparing the final survey with the survey containing the most recent upper cliff erosion event (> 300 $m^3$) for each section, it was possible to identify lean that was yet to result in collapse and test the point cloud's ability to forecast future cliff failure. In total, 14 separate instances were identified where lean had exceeded the 95 % confidence interval (Fig. 11). Conservatively, there were an additional 19 instances of lean identified that fell within the 95 % confidence interval but displayed tendencies of lean that have been observed previously. Section seven could be conceived as the most threatening area, as it contains three locations where lean exceeding the confidence interval have been detected (0.09 m, 0.16 m & 0.18 m).

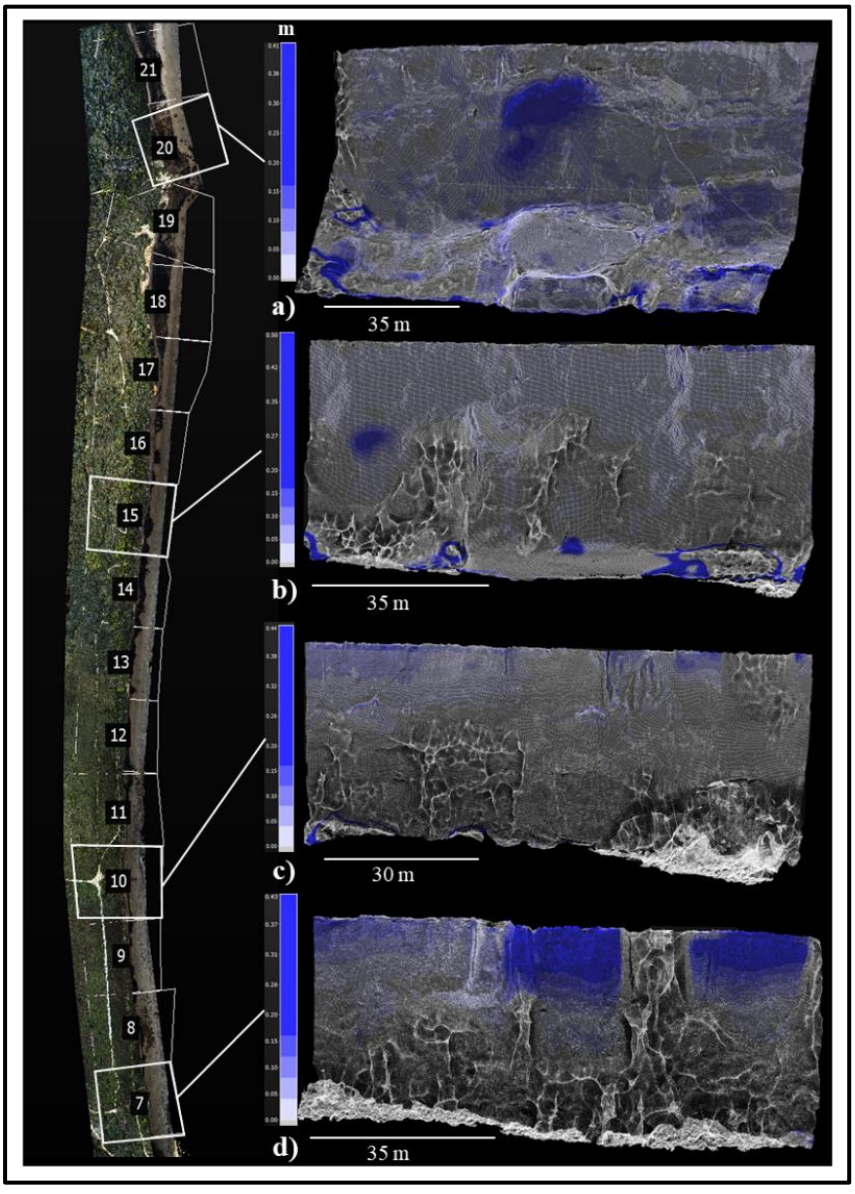


**Fig. 11:** M3C2 distance change output clouds showing sections where lean events have occurred but are yet to result in collapse.

https://doi.org/10.5194/egusphere-2024-659
Preprint. Discussion started: 19 April 2024


## 4. Discussion

### 4.1 Detection of Precursors to Collapse

In this study, point clouds have been effectively used to monitor cliff erosion over 50 months along a 1.5 km stretch of shoreline. This level of accuracy and precision, along with the ability to visualise 3D change, has proven to be able to track the precursors of cliff collapse, namely the initial seaward cleaving of large slabs of bedrock in soft carbonate mudstones. Previously, point clouds have been used to analyse the cliff face as one entity over smaller sites (Abellán et al., 2010, Earlie et al., 2018, Alessio and Keller, 2020, Gilham et al., 2019). However, this becomes less effective over larger sites due to a deterioration in the ability to measure incremental change caused by measurements being averaged over greater surface areas (Neverman et al., 2016). The ability to highlight localised retreat rates was provisioned by segmenting the cliff into 100 m sections in an alongshore direction and subsequently divided in half vertically based on the local geology. On average, segmentation permitted a LoD of 22 $m^3$ and 24 $m^3$ for the lower and upper halves the cliff respectively, across each 100 m section. This allowed the identification of at least 298 erosional events. If like other studies, the cliff face was treated as one entity, the LoD would increase to +/- 302 $m^3$ and the number of erosion events detected would decrease greatly. Segmentation also provided insight into localised retreat rates where sections observed to retreat in excess of 100 % greater than the mean annual retreat rate. This result is similar to Benjamin et al. (2020) who split over 20 km of Jurassic age mudstones, limestones and sandstones cliffs in North Yorkshire, UK into 100 m wide alongshore bins to allow the identification of localised measures of retreat. They also found that erosion rates contained spatial and temporal variations with different regions experiencing annual retreats from < 0.001 m, up to 1.63 m.

One observed benefit of the point cloud approach is a greater ability to detect the seaward displacement of the cliff face. In the case of Demons Bluff, this is caused by the expansion of cliff-top fractures that eventually result in moderate - high magnitude cliff collapse. Rock lean has been monitored previously using point clouds generated from terrestrial laser scans at Catalonia, Spain (Abellán et al. (2010)). Here, surveying of a small area of sea cliff (150 m wide, 25 m high) could detect block leaning that exhibited a displacement of 0.06 m prior to collapse (< 10 $m^3$). In this study, deformation could not be detected prior to failure of larger magnitude. They highlighted that the temporal resolution of survey was inadequate, and that deformation and the subsequent collapse likely occurred between the surveys. In this study, our method was able to emphasise the importance of high spatio-temporal resolution as the seaward displacement of cliff was detected prior to 75% (N = 8) of collapses > 300 $m^3$ within the upper cliff in sections 7 – 11. This was similar to Kromer et al. (2018) who utilised clusters of high temporal resolution sampling within different seasons and found a high success rate of 90 % in identifying deformation prior to larger collapses. However, in our study, outside of sections 7 – 11, precursory information was not detected for collapses of similar magnitude (> 300 $m^3$). This is likely due to the length and temporal resolution of the timeseries being smaller and not optimal for capturing the development of deformation prior to collapse and may benefit from a longer timeseries. Alternatively, as the baseline survey for some of the areas to the east did not occur until later in the study and there is potential that deformation had already occurred and was not detected, even if the timeseries was complete.
A high coincidence in identifying block lean in areas with complete timeseries illustrates that a temporal resolution of 6 – 8 weeks appears to be sufficient to identify deformation and gain an indication of a region's relative stability at Demons Bluff. Conversely, the lack of detection outside of sections 7 – 11 highlights that sustaining the timeseries is imperative for being able to identify deformation and potentially hazardous areas in the future. Kromer et al. (2018) also identified that the duration between deformation and eventual collapse ranged between 100s – 1000s of days. The timing between cliff deformation and collapse at Demons Bluff was shown to occur over a similar range. Tension Cracks were shown to exist behind the cliff top for the duration of the study (> 1000 days), while conversely, another instance of creep led to collapse at the same location where a high magnitude collapse event had occurred just 12 months earlier.

### 4.2 Comparison of Cliff Erosion Processes

The nature of retreat at Demons Bluff, like many other cliffs, is dominated by localised, episodic, and high magnitude events within the upper cliff (Dewez Thomas et al., 2013, Young et al., 2009, Letortu et al., 2015). However, this is not always the

https://doi.org/10.5194/egusphere-2024-659
Preprint. Discussion started: 19 April 2024


case, with Alesso and Keller (2020) finding upper cliff retreat to be more uniform year-round. They inferred the more constant nature of retreat was caused by wave-driven erosion of the cliff base that decreased cliff stability and permitted erosion to propagate up the cliff face. Their study encompassed much smaller cliffs (< 15 m in height) where small erosional events were more influential in driving cumulative retreat several magnitudes lower (< 0.08 m) than experienced in our study. Comparatively, at Demons Bluff, cliff heights ranged between 30 to 40 m and large upper cliff collapses drove higher cumulative retreat (max = 4.7 m). Small events (< 100 $m^3$) were also prevalent through time at Demons Bluff but contributed to a small amount of the total erosion (9%) which was dominated by high magnitude collapses (> 1,000 $m^3$, 71 %). Events between 100 $m^3$ - 1000 $m^3$ accounted for the remaining erosion and was primarily attributed to slabs detaching from the mid-cliff that caused the steepening and destabilisation of the cliff face (Young et al., 2009) until a proceeding cliff top failure restores slope stability.

In general, the drivers of cliff failure have been attributed to the weathering and weakening of rock masses from the exposure to marine and subaerial processes over long periods. Many studies of steep coastal cliffs have cited wave-driven under notching within the cliff toe as a primary cause of failure (Wilcock et al., 1998, Young and Ashford, 2008, Katz and Mushkin, 2013, Zelaya Wziątek et al., 2019, Dewez Thomas et al., 2013, Kogure et al., 2006, Letortu et al., 2015). Instances of the cliff toe undercutting the cliff top were absent at Demons Bluff. However, waves may still have an important role in slope destabilisation as they were observed to erode the talus deposits that protected the cliff base following collapse. Given that the cliffs are composed of highly erodible fine sediments, a lack of undercut may be attributed to a relatively weak geology that cannot support a sub-vertical slope over the entire cliff without resulting in cliff-top failure. Large collapses have also been shown to succeed cascades of smaller rockfalls and failures. For example, Gilham et al. (2019) recorded three successive failures that crossed the vertical extent of the cliff face within a small section of a coastal cliff over a four-month period. The final collapse was the largest and intersected the periphery of the two preceding failures. Similar processes were observed at Demons Bluff where slab detachments from the mid-cliff preceded high magnitude cliff-top failure that encompassed the same area as the initial detachment, and an instance where three large collapses (960 $m^3$, 4,260 $m^3$, and 1,900 $m^3$) intersected each other over a 24-month period. The latter of these also aligns with observations from Alesso and Keller (2020) who identified that new failure typically occurred in proximity with previous failures. Further study is required to determine the geotechnical and environmental factors that drive the formation and expansion of tension cracks along the crest of the cliffs in the Demons Bluff region.

## 5. Conclusion

This study has highlighted how a combination of point cloud analysis and high temporal resolution data collection can inform management decision making regarding hazardous coastal cliffs. In the future, with a greater understanding and confidence around the timing of failure, it may become possible to define areas at threat of collapse and flag environmental conditions that may induce failure to promote the safety of beach users and the preservation of coastal infrastructure. Future research priorities should be placed on the continued monitoring of the areas where lean was identified but collapse is yet to ensue. This may enhance our understanding into the timing of failure and the success of this method in forecasting the locations for collapse based on cliff deformation and help inform the development of a cliff collapse early warning system. Furthermore, this study focused on relatively large erosion events and highlighted the morphological processes of moderate-high magnitude (> 300 m) cliff failure. Future work should also be directed to identify if precursory cliff deformation can be detected prior to smaller failures and rockfalls (Benjamin et al., 2020, Gilham et al., 2019, Rosser et al., 2013). Subaerial and marine processes are known to affect rates of cliff retreat and morphological change. Future work should begin establishing whether relationships exist between weathering processes such as precipitation and wave action and cliff-face deformation and the timing of subsequent failure. This would further aid the development of an early warning system tool for management that may be applicable to other similar, neighbouring cliffs near Demon's Bluff that also experience high tourist visitation rendering the provision of safety of highest importance.

https://doi.org/10.5194/egusphere-2024-659
Preprint. Discussion started: 19 April 2024


## 6. Author Contribution

All authors designed the experiment. Data analysis was undertaken by TAD and all authors contributed to the preparation of the manuscript. DI and DK conceptualised the overall research program and secured fundings to support this work.

## 7. Data Availability

Data will be available on the Deakin Footprints repository but is not yet accessible. For reviewing, data can be downloaded via the following link:

https://filesender.aarnet.edu.au/?s=download&token=f9514076-5966-4afe-b84c-93f51b00272a

## 8. Competing Interests

The authors declare that they have no conflict of interest.

This project was supported by funding from the Victorian Government Department of Energy, Environment, and Climate Action and Victorian Coastal Monitoring Program (VCMP) through the Sustainability Fund, University of Melbourne and Deakin University. The citizen-scientists of the Anglesea region are thanked for their dedicated UAV flying. Appreciation is also extended to Parks Victoria and the Great Ocean Road Coasts and Parks Authority for supporting the mapping of Demons Bluff and for providing field assistance for data collection.

## 9. References

Abellán, A., Calvet, J., Vilaplana, J. M. , and Blanchard, J.: Detection and spatial prediction of rockfalls by means of terrestrial laser scanner monitoring, Geomorphology, 119, 162-171, https://doi.org/10.1016/j.geomorph.2010.03.016, 2010.

Alessio, P. and Keller, E. A.: Short-term patterns and processes of coastal cliff erosion in Santa Barbara, California, Geomorphology, 353, 106994, https://doi.org/10.1016/j.geomorph.2019.106994, 2020.

Benjamin, J., Rosser, N. J. , and Brain, M. J.: Emergent characteristics of rockfall inventories captured at a regional scale, Earth Surface Processes and Landforms, 45, 2773-2787, https://doi.org/10.1002/esp.4929, 2020.

Bezore, R., Kennedy, D. M. , and Ierodiaconou, D.: The evolution of sea cliffs over multiple eustatic cycles in high energy, temperate environments, Continental Shelf Research, 189, 10.1016/j.csr.2019.103985, 2019.

Bray, M. J. and Hooke, J. M.: Prediction of soft-cliff retreat with accelerating sea-level rise, Journal of Coastal Research, 453-467, 1997.

CloudCompare: (2.12), GPL Software [code], https://www.cloudcompare.org/, 2022.

Dewez Thomas, J. B., Rohmer, J., Regard, V. , and Cnudde, C.: Probabilistic coastal cliff collapse hazard from repeated terrestrial laser surveys : case study from Mesnil Val (Normandy, northern France), Journal of Coastal Research, 702-707, 2013.

Earlie, C., Masselink, G. , and Russell, P.: The role of beach morphology on coastal cliff erosion under extreme waves, Earth Surface Processes & Landforms, 43, 1213-1228, 10.1002/esp.4308, 2018.

https://doi.org/10.5194/egusphere-2024-659
Preprint. Discussion started: 19 April 2024


Esposito, G., Salvini, R., Matano, F., Sacchi, M., Danzi, M., Somma, R. , and Troise, C.: Multitemporal monitoring of a coastal landslide through SfM-derived point cloud comparison, The Photogrammetric Record, 32, 459-479, https://doi.org/10.1111/phor.12218, 2017.

Gilham, J., Barlow, J. , and Moore, R.: Detection and analysis of mass wasting events in chalk sea cliffs using UAV photogrammetry, Engineering Geology, 250, 101-112, https://doi.org/10.1016/j.enggeo.2019.01.013, 2019.

Gulyaev, S. and Buckeridge, J.: Terrestrial methods for monitoring cliff erosion in an urban environment, Journal of Coastal Research, 20, 871-878, 2004.

Hendrickx, H., Le Roy, G., Helmstetter, A., Pointner, E., Larose, E., Braillard, L., Nyssen, J., Delaloye, R. , and Frankl, A.: Timing, volume and precursory indicators of rock- and cliff fall on a permafrost mountain ridge (Mattertal, Switzerland), Earth Surface Processes and Landforms, 47, 1532-1549, https://doi.org/10.1002/esp.5333, 2022.

Ierodiaconou, D., Kennedy, D. M., Pucino, N., Allan, B. M., McCarroll, R. J., Ferns, L. W., Carvalho, R. C., Sorrell, K., Leach, C. , and Young, M.: Citizen science unoccupied aerial vehicles: A technique for advancing coastal data acquisition for management and research, Continental Shelf Research, 244, 104800, https://doi.org/10.1016/j.csr.2022.104800, 2022.

Katz, O. and Mushkin, A.: Characteristics of sea-cliff erosion induced by a strong winter storm in the eastern Mediterranean, Quaternary Research, 80, 20-32, 10.1016/j.yqres.2013.04.004, 2013.

Kogure, T., Aoki, H., Maekado, A., Hirose, T. , and Matsukura, Y.: Effect of the development of notches and tension cracks on instability of limestone coastal cliffs in the Ryukyus, Japan, Geomorphology, 80, 236-244, 2006.

Kromer, R. A., Rowe, E., Hutchinson, J., Lato, M. , and Abellán, A.: Rockfall risk management using a pre-failure deformation database, Landslides, 15, 847-858, 2018.

Lague, D., Brodu, N. , and Leroux, J.: Accurate 3D comparison of complex topography with terrestrial laser scanner: Application to the Rangitikei canyon (N-Z), ISPRS Journal of Photogrammetry and Remote Sensing, 82, 10-26, https://doi.org/10.1016/j.isprsjprs.2013.04.009, 2013.

Letortu, P., Costa, S., Maquaire, O., Delacourt, C., Augereau, E., Davidson, R., Suanez, S. , and Nabucet, J.: Retreat rates, modalities and agents responsible for erosion along the coastal chalk cliffs of Upper Normandy: The contribution of terrestrial laser scanning, Geomorphology, 245, 3-14, 2015.

Letortu, P., Jaud, M., Ammann, J., Le Dantec, N., Delacourt, C., Grandjean, P., Costa, S., Maquaire, O. , and Davidson, R.: Examining high-resolution survey methods for monitoring cliff erosion at an operational scale, GIScience and Remote Sensing, 55, 457-476, 10.1080/15481603.2017.1408931, 2018.

Li, Y., Liu, P., Li, H. , and Huang, F.: A comparison method for 3D laser point clouds in displacement change detection for arch dams, ISPRS International Journal of Geo-Information, 10, 184, 2021.

Lim, M., Rosser, N. J., Allison, R. J. , and Petley, D. N.: Erosional processes in the hard rock coastal cliffs at Staithes, North Yorkshire, Geomorphology, 114, 12-21, https://doi.org/10.1016/j.geomorph.2009.02.011, 2010.

Limber, P. W., Barnard, P. L., Vitousek, S. , and Erikson, L. H.: A Model Ensemble for Projecting Multidecadal Coastal Cliff Retreat During the 21st Century, Journal of Geophysical Research: Earth Surface, 123, 1566-1589, https://doi.org/10.1029/2017JF004401, 2018.

Liu, J., Meucci, A., Liu, Q., Babanin, A. V., Ierodiaconou, D. , and Young, I. R.: The wave climate of Bass Strait and South-East Australia, Ocean Modelling, 172, 101980, https://doi.org/10.1016/j.ocemod.2022.101980, 2022.

Mancini, F., Castagnetti, C., Rossi, P., Dubbini, M., Fazio, N. L., Perrotti, M. , and Lollino, P.: An Integrated Procedure to Assess the Stability of Coastal Rocky Cliffs: From UAV Close-Range Photogrammetry to Geomechanical Finite Element Modeling, Remote Sensing, 9, 1235, 2017.

https://doi.org/10.5194/egusphere-2024-659
Preprint. Discussion started: 19 April 2024


Neverman, A. J., Fuller, I. C. , and Procter, J. N.: Application of geomorphic change detection (GCD) to quantify morphological budgeting error in a New Zealand gravel-bed river: A case study from the Makaroro river, Hawke's bay, Journal of Hydrology (New Zealand), 45-63, 2016.

Pucino, N., Kennedy, D. M., Carvalho, R. C., Allan, B. , and Ierodiaconou, D.: Citizen science for monitoring seasonal-scale beach erosion and behaviour with aerial drones, Scientific reports, 11, 1-17, 2021.

Rohmer, J. and Dewez, T.: On the deviation of extreme sea-cliff instabilities from the power-law frequency-volume distribution : practical implications for coastal management, Journal of Coastal Research, 1698-1703, 2013.

Rosser, N. J., Brain, M. J., Petley, D. N., Lim, M. , and Norman, E. C.: Coastline retreat via progressive failure of rocky coastal cliffs, Geology, 41, 939-942, 10.1130/g34371.1, 2013.

Scaioni, M., Roncella, R. , and Alba, M. I.: Change detection and deformation analysis in point clouds, Photogrammetric Engineering & Remote Sensing, 79, 441-455, 2013.

Shalaby, M. R., Irwan, M. I. I. b. H., Osli, L. N. , and Islam, M. A.: Geochemical characteristics and depositional environments of the Narimba Formation source rock, Bass Basin, Australia, Journal of Petroleum Exploration and Production Technology, 10, 3207-3225, 10.1007/s13202-020-00992-4, 2020.

Smith, G. L. and Zarillo, G. A.: Calculating long-term shoreline recession rates using aerial photographic and beach profiling techniques, Journal of coastal research, 111-120, 1990.

Terefenko, P., Paprotny, D., Giza, A., Morales-Nápoles, O., Kubicki, A. , and Walczakiewicz, S.: Monitoring Cliff Erosion with LiDAR Surveys and Bayesian Network-based Data Analysis, Remote Sensing, 11, 843, 2019.

Theodore, P., Thomas, H., Adonis, V., Theophanis, K., Emmanouel, O. , and Charalampos, D.: Erosion status of a sea cliff promontory bounding an ecologically important beach, Journal of Coastal Conservation (Springer Science & Business Media B.V.), 24, 1-5, 10.1007/s11852-020-00756-6, 2020.

Wilcock, P. R., Miller, D. S., Shea, R. H. , and Kerkin, R. T.: Frequency of effective wave activity and the recession of coastal bluffs: Calvert Cliffs, Maryland, Journal of Coastal Research, 256-268, 1998.

Young, A. P. and Ashford, S. A.: Instability investigation of cantilevered seacliffs, Earth Surface Processes and Landforms, 33, 1661-1677, https://doi.org/10.1002/esp.1636, 2008.

Young, A. P. and Carilli, J. E.: Global distribution of coastal cliffs, Earth Surface Processes and Landforms, 44, 1309-1316, https://doi.org/10.1002/esp.4574, 2019.

Young, A. P., Flick, R. E., Gutierrez, R. , and Guza, R. T.: Comparison of short-term seacliff retreat measurement methods in Del Mar, California, Geomorphology, 112, 318-323, https://doi.org/10.1016/j.geomorph.2009.06.018, 2009.

Young, A. P., Flick, R. E., O'Reilly, W. C., Chadwick, D. B., Crampton, W. C. , and Helly, J. J.: Estimating cliff retreat in southern California considering sea level rise using a sand balance approach, Marine Geology, 348, 15-26, https://doi.org/10.1016/j.margeo.2013.11.007, 2014.

Zelaya Wziątek, D., Terefenko, P. , and Kurylczyk, A.: Multi-Temporal Cliff Erosion Analysis Using Airborne Laser Scanning Surveys, Remote Sensing, 11, 2666, 2019.